Landscape Characterization of the Cauvery Basin, India using Geomorphic Indices Derived from the Digital Elevation Model

Sudhanshu Raghubanshi[1]*, Ritesh Agrawal[1], and Dhani Ram Rajak[1]
[1]Space Applications Centre (SAC), ISRO, Ahmedabad, 380015, Gujarat, India
*Corresponding author email: sraghubanshi@gmail.com

(Received on 28 May 2025; In final form on 14 August 2025)

DOI: *https://doi.org/10.58825/jog.2025.19.2.257*.

Abstract: Landscape characterization is essential for deciphering geomorphic evolution, resource potential, and sustainable management in river basins. While geomorphic indices are commonly used for quantifying terrain and assessing erosion, their integrated application with landform features remains underexplored. This study offers a comprehensive landscape assessment of the Cauvery River Basin, India, by integrating geomorphic indices with landform features to study spatial patterns of fluvial erosion. Using Shuttle Radar Topography Mission (SRTM-30 m) data, three geomorphic indices-Hypsometric Integral (HI), Hack's Stream-Length Gradient (SL) Index, and Normalized Channel Steepness (K_{sn}) Index-were computed across six sub-basins, along with landform classification. The HI values ranged from 0.11 to 0.27, indicating varied stages of landscape development, with the Shimsha sub-basin showing the highest HI (0.27), and the Kabini, Noyil, and lower Cauvery basins the lowest (0.11–0.12), suggesting mature, eroded terrains. Knickpoints analysis showed intense incision in the Bhavani basin (3162 knickpoints), supported by high K_{sn} values (90), and high SL values (up to 160,884 gradient meters), particularly around waterfalls and dams shaped by lithological controls. Clustering of knickpoints at elevations between 0-120 m above sea level, suggests that Quaternary eustatic base-level fall triggered a phase of river rejuvenation across the basin. Landform classification shows plains dominate (52-89 % areal coverage), especially in lower sub-basins, while ridge and deeply incised streams show more active erosion zones. This integration of geomorphic indices and landforms shows a framework for linking fluvial erosion to sea-level history, providing insights into past geomorphic responses, lithological controls over river basin evolution, and implications for sustainable land and water resource management.

Keywords: Landscape, geomorphic indices, hypsometric analysis, Hack index, base-level fall.

1. Introduction

Morphometry is a valuable aspect for inferring the stages of erosion within various watersheds (Keller and Pinter, 2002, Bull 2007, Anderson and Anderson, 2010, Burbank and Anderson, 2011). Additionally, morphometry facilitates the evaluation of geomorphic characteristics and the influence of lithology on watersheds (Das 2018). Historically, geomorphometric analysis of drainage basins relied on manual methods, which were characterized as tedious, labor-intensive, and time-consuming (Horton 1945, Coates 1958). However, advancements in computer technology, particularly the integration of Geographical Information Systems (GIS) and the application of remote sensing alongside various digital elevation datasets, have revolutionized geomorphometry (Pike 1999). This integration has significantly enhanced the computation of different geomorphometric properties of the Earth's surface, rendering the process faster and more accurate than before (Das et al., 2017, Das and Pardeshi, 2018a, b).

Geomorphic indices, derived from topographic data that is collected through satellite data, aerial photographs, topographic maps, and field-based studies, provide insights into the landscape development (Das 2018). Assessing the landscape development of a specific terrain involves examining the influence of climate, tectonics, geology, and lithology. The hypsometric integral (HI) (Strahler 1952), stream length (SL) index (Hack 1973), and normalized channel steepness index (k_{sn}) are among the geomorphic indices utilized to evaluate landscape development of a particular basin (Schumm 1956, Keller and Pinter, 2002, Wobus et al., 2006, Perez-Peña et al., 2009a, Kirby and Whipple, 2012, Perron and Royden, 2013, Mudd et al., 2014).The hypsometric curve (HC) of a watershed illustrates the distribution of relative area above or below a specified elevation (Strahler 1952), depicted by plotting the proportions of total basin area against height (Langbein 1947, Strahler 1952). The morphology of the HC also indicates the lithological, climatic, and tectonic factors influencing the basin (Moglen and Bras, 1995, Willgoose and Hancock, 1998, Huang and Niemann, 2006). Regions characterized by slightly eroded landscapes exhibit convex curves, while moderately eroded areas show S-shaped curves, and highly eroded regions display concave curves (Strahler 1952).

Fluvial processes are the most influential geomorphic agents, shaping landscapes through the effects of melted snow or rainfall (Das and Pardeshi, 2018a). The quantification of drainage and the study of their patterns play a crucial role in analyzing landscape development in fluvial-impacted topography. Drainage channel studies were initiated by Horton (1932, 1945), with his techniques further utilized by numerous researchers (Strahler 1957, 1964, Schumm 1956, Gregory 1966, Manu and Anirudhan, 2008, Sreedevi et al., 2005, Thomas et al., 2011, Dusan et al., 2017, Kumar et al., 2015, Das and Pardeshi, 2018a). In studying the lithological and structural control over a specific drainage basin, the longitudinal profile of a river often produces more elaborative results compared to morphometric analyses of

the basin. This is because the river channel is the most sensitive feature in fluvial-generated landscapes, preserving evidence of structural changes in the geological past and terrain deformation (Das et al., 2018).

Knickpoints, characterized by discrete changes in river gradient derived from the longitudinal profile of a river, are useful parameters for identifying the topographic evolution of terrain and understanding climatic and tectonic controls (Bishop et al., 2005). A knickzone or knickpoint, often observed in bedrock channels, represents a significantly steeper segment compared to adjacent segments of a longitudinal profile (Wohl et al., 1999, Zaprowski et al., 2001, Hayakawa and Oguchi, 2006, Sun et al., 2016). This parameter is crucial for understanding river adjustment in response to transient or intrinsic perturbations. Vertical knickpoints can result from rapid base level falls (e.g., tectonic, eustatic, river capture), lithological contrasts across vertical and horizontal contacts, and abrupt increases in discharge across tributary junctions (Bishop et al., 2005). The phenomena responsible for knickpoint and knickzone formation include changes in base level, tectonic uplift, lithological differences, volcanic activity, and glacial retreat (Lewis 1945, García et al., 2004, Miller 1991, Alexandrowicz 1994, Hayakawa and Oguchi, 2006, Das et al., 2018, Gailleton et al., 2019).

Knickpoints can be identified using the Hack index. Hack (1973) developed the SL index, which represents the ratio of slope to length or stream-length gradient, to delineate breakpoints in the slope of longitudinal river profiles. By employing the SL index, one can identify "anomalous" segments of stream sections, which are then used to assess whether the river is in geomorphological equilibrium conditions or not (Seeber and Gornitz, 1983, McKeown et al., 1988, Merrits and Hesterberg, 1994, Marple and Talwani, 1993, Etchebehere et al., 2004, Martinez et al., 2011). The SL Index method enables the study of the differential erosion of a particular basin and the structural and lithological controls over it, as well as the deformation imposed by neotectonic activity (Etchebehere et al., 2006).

The present study integrates the geomorphic indices with landform features, which remains underexplored. Landforms refer to specific geomorphic features on the Earth's surface, encompassing minor features like individual hills and valleys to large-scale features such as plains and mountains (Blaszczynski 1997). Landform holds significant importance across various fields, including precision agriculture, vegetation mapping, prediction of soil properties (Schmidt and Hewitt, 2004), and lithology mapping. The availability of different digital elevation models has provided opportunities for landform classification (Meybeck et al., 2001). It has been conducted using various automated techniques (Schmidt and Hewitt, 2004, Saadat et al., 2008), morphometric parameters employing filter techniques, multivariate statistics, and cluster analysis (Dikau 1989, Adediran et al., 2004), as well as contour maps (Dikau et al., 1991). Guisan et al., (1999) developed an automated landform classification technique using the Topographic Position Index (TPI) method, further refined by Weiss (2001) and utilized by Jenness (2006).

In the current study, three types of geomorphic indices (HI, SL index, and K_{sn} index) were calculated to characterize the landscape of the Cauvery basin. The aim was to establish a relationship between these indices and landform features to assess the influence of extracted geomorphic indices on the topography.

2. Study Area and Data Used

The study area encompasses the Cauvery basin in India (Figure 1), where geomorphic indices are computed for landscape characterization and development analysis. The analysis was conducted using Shuttle Radar Topography Mission (SRTM) Digital Elevation Model (DEM) data with a resolution of 30 meters (Figure 1). Additionally, high-resolution images from Google Earth were employed for validation purposes, particularly in locations exhibiting high values of geomorphic indices such as SL and $K_{sn.}$ The Cauvery basin is divided into three parts: the upper, middle, and lower basins. The upper part passes through Karnataka state, while the middle part passes through Karnataka, Kerala, and Tamil Nadu. The lower part covers parts of Tamil Nadu and the union territory of Puducherry. Originating at an elevation of 1342 m near the village of Kodagu in Karnataka, the Cauvery River has several tributaries (Central Water Commission, 1989). The upper basin receives precipitation from the southwest monsoon, while the northeast monsoon plays a major role in draining the lower basin, making the Cauvery River perennial. Covering over a distance of 800 kilometers in its course, with a catchment area of approximately 83,000 km^2, the Cauvery River flows eastward and discharges its water into the Bay of Bengal. The Cauvery basin was divided into six sub-basins using pour points along the main channel (Figure 1). The upper part of the Cauvery River contains the Hemavathi major river basin, with Yagachi and Lakshmantirtha as minor tributaries. The middle region includes the Kabini, Shimsha, Bhavani, and Noyil major river basins, along with minor tributaries such as Gundal, Suvarnavathy, Arkavathy, Moyar, Sarabenga, Amaravathi, Nangani, and Kodavanar etc.

The lower region denotes the final part of the Cauvery River before it empties into the Bay of Bengal. The highest order of stream 7 was observed in this basin (Figure 5). The Cauvery basin comprises various geological ages, including Archaean, Archaean-Proterozoic, Quaternary, Miocene-Pliocene etc. (Figure 2). Predominantly, Precambrian cratonic rocks such as the Dharwars, Peninsular granitic gneiss, Charnockites, and the Closepet granite are dominant rock formations in this basin (Stalin and Achyuthan, 2014).

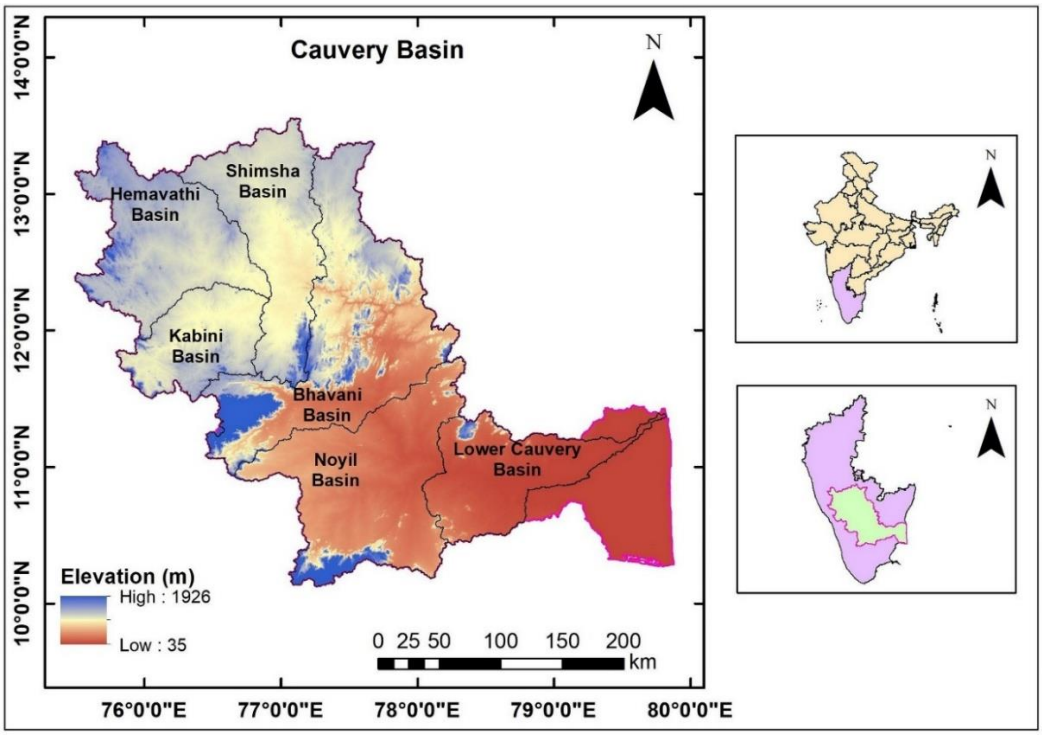

Figure 1. Location map of the study area

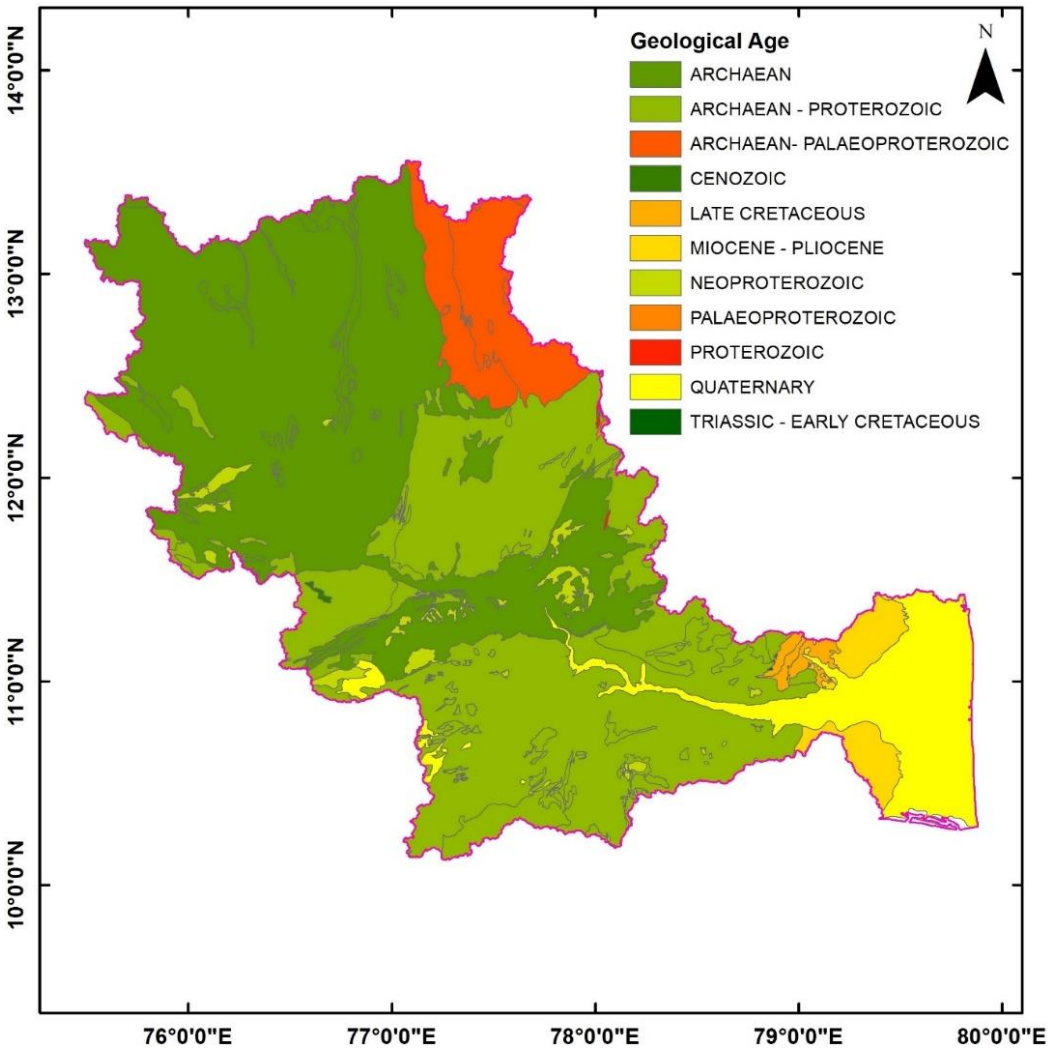

Figure 2. Geological age map

3. Methodology

To achieve the objective, three geomorphic indices, such as hypsometric integral (HI), Hack (SL) index, and normalized channel steepness (K_{sn}) index were computed, which are explained below. These parameters were extracted using SRTM 30 m DEM as input. This DEM was preprocessed using standard hydrological (spatial analyst) tools in ArcGIS 10.5. This included filling sinks, generating flow direction and flow accumulation grids, and extracting the drainage network. Sub-basins were delineated using pour points, ensuring accurate stream and watershed representation for geomorphic analysis. This allowed for the comprehensive assessment of the basin's geomorphic characteristics and characterization of its topography.

3.1 Hypsometric Integral

The hypsometric curve (HC) of a specific drainage basin is shaped by the hypsometric integral (HI), defined as the area under the HC (Strahler 1952). The calculation of HI values adopting a zonal procedure approach to assign mean, maximum, and minimum elevations to each sub-basin area (Jaiswara et al., 2020), as per the formula:

$$HI = (E_{mean} - E_{min}) / (E_{max} - E_{min}) \quad (1)$$

Here, E_{min}, E_{mean}, and E_{max} represent the minimum, mean, and maximum elevations of the drainage basin, respectively. The resulting HI values lies in the range of 0 to 1, where a value close to 0 indicates a highly eroded and dissected region (old topography), while a value close to 1 indicates a slightly eroded region (young topographic region) [Pedrera et al., 2009].

In this study, the percentage hypsometric method was employed (Jaiswara et al., 2020) for hypsometric analysis. This method involves plotting two ratios, the relative elevation ratio (h/H) and the relative area ratio (a/A), against each other on a graph. The range of HI values can be utilized to estimate the stages of the watershed (Miller 1953) as follows: **A.** HI ≥ 0.6 (youthful stage), **B.** 0.35 ≤ HI< 0.6 (Equilibrium or mature stage), and **C.** HI< 0.35 (Old stage). Watersheds in the youthful stage are more prone to erosion compared to those in the mature or old stages. However, watersheds in the mature stage are more prone to erosion than those in the old stage.

3.2 Hack Index

The Hack index establishes the relationship between the slope and length of a stream (Hack 1973).

Hack assumes the stream profile to be a straight line (Figure 3), given by the equation:

$$h = c - k.\log_e(l) \quad (2)$$

Where h and l denote the elevation and stream length from the drainage divide at the point of calculation, and c and k are constants. The slope at the point of calculation is given by the derivative of this equation:

$$S = \Delta h/\Delta l = k/l \quad (3)$$

Where S represents the slope. The Hack index k is calculated using:

$$k = (\Delta h/\Delta l) \times l \quad (4)$$

k is known as the Hack or stream-length gradient (SL) index. In this study, the SL index was calculated using the knickpoint finder tool developed by Queiroz et al., 2015, in Python and implemented in the ArcGIS environment. An elevation interval of Δh= 30 m was taken for the calculation.

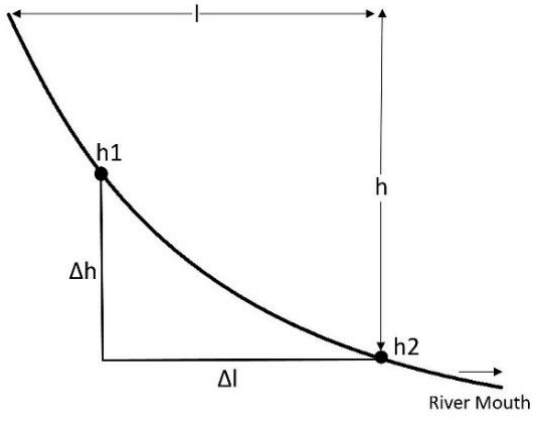

Figure 3. Procedure for calculating the Hack index along the longitudinal profile of a river

3.3 Normalized Channel Steepness Index

A sudden break in slope, caused by lithological contrasts or the presence of faults, leads to the adjustment of a stream to a new equilibrium condition, which can be expressed mathematically as (Howard and Kerby, 1983, Howard 1994, Whipple et al., 2000):

$$\frac{dz}{dt} = U - E \quad (5)$$

Where z represents elevation, t denotes time, U signifies upliftment, and E denotes erosion rates. The erosion rate E is further given by:

$$E = KA^m S^n \quad (6)$$

Where K is the erosion efficiency parameter dependent on sediments and rock strength, A represents the upstream drainage area, S corresponds to channel slope, and m and n are constants determined by erosion conditions, hydraulic geometry, and basin hydrology (Howard et al., 1994, Whipple and Tucker, 1999, Whipple et al., 2000). Combining equations (5) and (6),

$$\frac{dz}{dt} = U - KA^m S^n \quad (7)$$

The variation in elevation with time governs the value dz/dt. In a steady-state condition, where there is no change in landscape (topography), the rates of upliftment and erosion are equal, gives dz/dt=0 (Kirby and Whipple, 2012). Therefore,

$$U = KA^m S^n \quad (8)$$

Rearranging equation (8),

$$S = \left(\frac{U}{K}\right)^{1/n} A^{-m/n}$$

$$S = k_s A^{-\theta} \quad (9)$$

Where $k_s = (U/K)^{1/n}$, which is the steepness index of the profile, and $\theta = \frac{m}{n}$, which is the concavity of the profile.

The values of m and n can be determined by regression analysis of S and A (Howard 1994, Montgomery et al., 1996, Schoenbohm et al., 2004, Snyder et al., 2000, Whipple 2004, Wobus et al., 2006).

A large variation in the value of m was observed due to small changes in the value of n. To overcome this limitation and correlate watersheds of different sizes and shapes, a normalized channel steepness index (K_{sn}) was calculated using concavity (θ_{ref}) [Wobus et al., 2006]:

$$S = k_{sn} A^{-\theta ref} \quad (10)$$

For a steady-state channel, the value of θ lies between $0.4 \leq \theta \leq 0.5$ (Wobus et al., 2006, Kirby and Whipple, 2012). The average of all the values of θ is represented by θ_{ref}.

The K_{sn} was calculated using software developed by Jaiswara et al., (2020) in MATLAB, with θ_{ref} set as 0.45 by regression analysis of S and A (Snyder et al., 2000). It was calculated with a window of 0.5 km to analyze the lithological effect along the channel (Jaiswara et al., 2020).

3.4 Landform Classification

For landform classification, the Topographic Position Index (TPI) [Guisan et al., 1999] was used, which was further modified by Weiss (2001) and Jenness (2006). The integrated analysis of the TPI and slope position classification gives ten different classes of landform features. TPI calculates the elevation of each cell of a digital elevation model relative to the mean elevation of the specified neighborhood around that cell. A value greater than zero represents regions higher than their surroundings, less than zero represents regions lower than their surroundings, and a value close to zero represents regions at the same elevation as their surroundings or saddle regions. The TPI values can be classified into slope position classes to compute the slope value for each point based on different threshold values. Landscape classification into various landform classes depends on scale parameters such as neighborhood size and shape (Mokarram and Seif, 2014). In this study, a combination of TPI values with low (7 & 12) and high (32 & 37) neighborhood sizes produced different types of landforms (Weiss 2001). The chosen threshold for plain areas (leveling in degrees) was 5^0, with a standard deviation threshold of ±1, which provided the optimal classification of landform features in the selected study area.

4. Results and Discussion

Three key geomorphic indices, HI with HC, SL, and K_{sn} indices, were estimated to understand the erosional status and landscape development history over the Cauvery basin, India. To investigate how these indices affected the topography of the basin, a relationship between the obtained geomorphic indices and landform features was further analyzed.

4.1 Hypsometric Analysis

The hypsometric analysis was used to estimate the HI, area, and max-min-mean elevation within the sub-basins (Table 1) and corresponding hypsometric curves (Figure 4). It was observed that the Bhavani basin emerged as the largest sub-basin, covering an area of 21,842 km^2, while the Kabini basin was the smallest, with an area of 7,649 km^2. The maximum elevation was observed in the Bhavani basin, 2,634 m. The Hemavathi basin exhibited the highest mean elevation (896 m), while the lower Cauvery basin had the lowest (155 m) (Table 1). The Kabini and lower Cauvery basins exhibited HI values of 0.11 and the Noyil basin had a value of 0.12. However, the Hemavathi and Bhavani basins displayed HI values of 0.22, while the Shimsha basin had the highest value of 0.27. The Table 1 represented significant variation in HI values across the different sub-basins of the Cauvery River. These variations indicate distinct differences in erosional activity among the basins. The lower HI values for the Kabini, Noyil, and lower Cauvery basins indicate highly eroded and dissected topography compared to the Hemavathi, Shimsha, and Bhavani basins, which have relatively higher HI values. The greater uneroded volume in the Hemavathi, Shimsha, and Bhavani basins suggests the potential for increased erosional activity in the future compared to other basins.

The areal distribution analysis of all six sub-basins were carried out for the understanding of the area coverage with respect to elevation distribution. Elevation values were classified into 20 classes using equal intervals and corresponding areas (percentage) were estimated (Table 2).

From Table 2, it was observed that almost all the sub-basins cover around 95% areal coverage in 40 % elevation range except in the Bhavani basin. It was also observed that the HI of the Hemavathi and Bhavani basins is 0.22

(Table 1), but the elevation distribution is different as shown in their HC (Figure 4). The analysis shows that the Hemavathi basin covers a smaller area in the lower range (18% area in covering 15% elevation range), while the Bhavani basin covers 37.6 % areal coverage in 15% elevation range. However, the Hemavathi basin compensates by covering 67% area as compared to 29% area covered by the Bhavani basin in the middle elevation range of 15-30%. The Hemavathi basin area is more evenly spread across middle elevations, while the Bhavani basin area spread shows a mix of low and middle elevations. For this, their HC would differ (Figure 4), despite of same HI values, indicating their different erosion stages or landscape maturity. The HI of the Kabini, Noyil, and lower Cauvery basins have similar values (0.11, 0.12, and 0.11), while elevation distribution also behaves similarly in these basins with a marginal increase in areal coverage (61%) in the Noyil basin in lower range (0-10% elevation range) as compared to the Kabini and lower Cauvery basins having coverage of around 47% and 57% (0-10% elevation range).

The HC for these sub-basins would be more convex (Figure 4), indicating a more gradual slope with more area at lower elevations, shows their flatter terrain. The Shimsha basin has different characteristics from other sub-basins having the highest HI (0.27). The elevation distribution shows that it covers a very small area 1.5% up to 15% elevation range. However, the maximum extent around 90% of this basin is covered by the middle range (15-35%), which indicates a relatively youthful landscape with less erosion.

This analysis demonstrates how the HI values, a measure of landscape maturity, can be linked to the areal distribution of elevations within a sub-basin. Equal HI values may arise from different distributions, same mean elevation relative to range, but different spreads, suggesting different landscape processes (e.g., Hemavathi and Bhavani basins). Further, higher HI values correlate with a significant portion of the area at higher elevations (e.g., Shimsha basin). Similar HI values indicate similar stages of landscape evolution with minor differences in elevation distribution (e.g., Kabini, Noyil, and lower Cauvery basins). In addition, the concave shape of the HC (Figure 4) suggests that all sub-basins are in their old stages and represent highly eroded regions in landscape characterization.

4.2 Knickpoints Analysis

Landscape characterization was evaluated with slope break (knickpoints) analysis along the stream channels, which were determined using the SL index. The SL classes were chosen based on natural breaks in the data distribution to capture gradational changes in knickpoints. The calculated values of this index are presented in Table 3, and the spatial distribution of knickpoints is illustrated in Figure 5. The table contains total number, distribution, and maximum value of SL, and the range values of the K_{sn}. The Bhavani basin exhibited the maximum number of knickpoints, with 3162, followed by the Noyil basin with 1260. However, the lower Cauvery basin had the minimum number of knickpoints at 257, followed by the Kabini basin with 279. In the Bhavani basin, knickpoints spread across multiple elevation ranges, with the highest SL value recorded at 160,884 gradient meters, followed by the Shimsha (61,545 gradient meters), Noyil (15,548 gradient meters), lower Cauvery (11,530 gradient meters), and Hemavathi (1951 gradient meters) basins.

Table 1. Hypsometric analysis

Basins	Area (Sq. Km.)	Maximum Elevation (m)	Minimum Elevation (m)	Mean Elevation (m)	HI
Hemavathi	13280	1814	639	896	0.22
Kabini	7649	2030	638	797	0.11
Shimsha	12520	1813	408	784	0.27
Bhavani	21842	2634	156	704	0.22
Noyil	17739	2542	101	393	0.12
Lower Cauvery	9698	1403	0	155	0.11

It was observed that, the Bhavani basin contained three knickpoints in the range of 62,000-161,000; no other basins exhibited knickpoints within this range. In addition, the Bhavani basin contained the highest number of knickpoints across all ranges, followed by the Noyil basin, which contained the second-highest number. The Kabini basin did not contain any knickpoints in the range of >= 1000-2000, while the Hemavathi basin had no knickpoints in the range of >= 2000-4000. The Kabini basin exhibited only one knickpoint in the 500-1000 range, with the rest between 30 and 500. The Hemavathi basin contained four knickpoints, each in the 500-1000 and 1000-2000 ranges, with the remaining knickpoints between 30 and 500. The minimum number of knickpoints in the 30-500 range was observed in the lower Cauvery basin (210), followed by the Kabini basin (278). The Shimsha, Noyil, and lower Cauvery basins contained knickpoints across all ranges except the highest range, although their numbers were fewer compared to the Bhavani basin.

The distribution of knickpoints shows the topographic variability and erosion patterns within the basin. It was observed that the density of knickpoints showed a strong correlation with the nature of the topography, particularly the undulating terrain. The Bhavani basin displayed the highest density of knickpoints (Figure 5), indicating relatively rugged topography compared to the other basins. Higher knickpoint densities were observed in the upper region of the Noyil, the lower Cauvery, and the lower region of the Shimsha basins, suggesting rugged or undulating terrain in these areas.

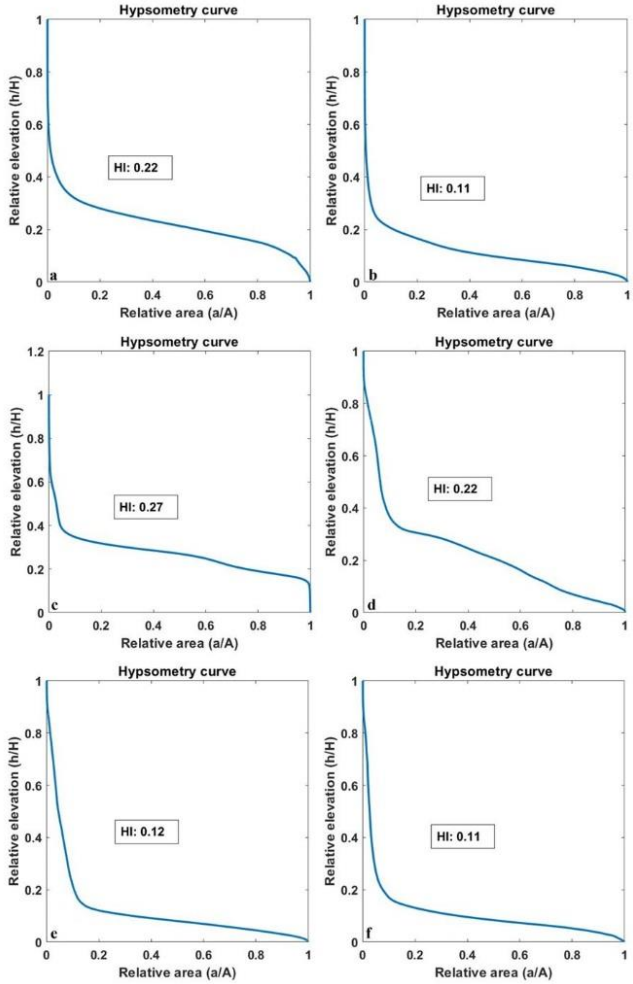

Figure 4. Hypsometric curves for the six sub-basins: **a)** Hemavathi, **b)** Kabini, **c)** Shimsha, **d)** Bhavani, **e)** Noyil, and **f)** Lower Cauvery

Table 2. Areal distribution analysis with elevation

Elevation (%)	Hemavathi Basin Area (%)	Kabini Basin Area (%)	Shimsha Basin Area (%)	Bhavani Basin Area (%)	Noyil Basin Area (%)	Lower Cauvery Basin Area (%)
0-5	2.1047	10.7350	0.0631	12.2211	17.6170	12.4333
5-10	4.7624	35.2511	0.0846	14.9410	43.3176	44.2503
10-15	11.2813	26.8579	1.2918	10.4280	24.8814	27.7245
15-20	23.9890	14.5312	20.6059	10.2652	3.4929	7.4862
20-25	24.8531	7.7420	16.9003	12.8699	1.5138	2.5016
25-30	18.6647	2.2157	28.3636	15.6171	1.0806	1.1143
30-35	7.5176	0.9406	22.4357	12.4283	0.8776	0.6990
35-40	3.0649	0.5524	5.7275	2.6098	0.9060	0.5247
40-45	1.6820	0.3774	0.9858	1.4367	0.8715	0.3626
45-50	0.9347	0.2743	0.6738	0.7989	0.9256	0.2934
50-55	0.5398	0.2015	0.8180	0.5752	0.6414	0.2800
55-60	0.2704	0.1460	0.9692	0.5784	0.4366	0.2576
60-65	0.1514	0.0657	0.5330	0.6981	0.4840	0.2263
65-70	0.1117	0.0401	0.2243	0.9261	0.4961	0.2081
70-75	0.0379	0.0270	0.1289	1.0102	0.5472	0.3058
75-80	0.0213	0.0170	0.0894	1.0052	0.5540	0.3767
80-85	0.0088	0.0128	0.0582	0.9734	0.5441	0.4978
85-90	0.0031	0.0084	0.0312	0.4935	0.5435	0.3350
90-95	0.0012	0.0026	0.0143	0.1105	0.2259	0.1136
95-100	0.0002	0.0012	0.0014	0.0133	0.0430	0.0095

However, lower knickpoint densities were observed in the Hemavathi, the Kabini, the upper part of Shimsha, the lower part of the Noyil, and the lower Cauvery basins, indicating less undulating topography in these locations. The total number of knickpoints in each basin also reflects the nature of the topography. The Bhavani basin, characterized by highly rugged terrain compared to other basins, contained the highest number of knickpoints (3162), followed by the Noyil basin (1260). Conversely, all other basins had total knickpoint counts of less than 500, indicating relatively less rugged terrain. This spatial distribution of knickpoints provided insights into the lithological controls on the basin's topography, highlighting areas of relatively active erosion and landscape instability

It was observed that knickpoint across the Cauvery basin shows concentration within the 0-120 m elevations range above present sea level (Figure 5). This elevation interval aligns with the estimated sea-level low stand of approximately 100-120 m during the last glacial maximum (~20,000 years ago) [Lambeck et al., 2014]. The spatial coincidence between this knickpoint clustering suggests a basin-wide response to a major base-level fall. Such situation shows that river profiles across the basin were destabilized and began adjusting to the lowered base level, initiating an upstream-propagating incision, which shows fluvial rejuvenation (Nagendra and Reddy, 2017). This rejuvenation, likely triggered by Quaternary sea-level fall (Lambeck et al., 2014), points to a significant influence on fluvial erosion within the basin. This interpretation highlights that the current geomorphic structure of the Cauvery basin is not only a product of tectonics or lithology, but also reflects the imprint of past global sea level fluctuations (Ramkumar et al., 2003)

4.3 Normalized Channel Steepness Index Profile Analysis

In all six sub-basins, the K_{sn} was calculated for the streams containing the highest values of knickpoints, and their steepness profiles were generated (Figure 6). K_{sn} analysis was used to study the stream channel morphology to identify areas of differential erosion. Variations in K_{sn} values were observed, indicating the degree of incision and landscape rejuvenation. The maximum K_{sn} value range was observed for the Bhavani River (75-90) shows active incision, while the minimum was found for the lower Cauvery (20-25) (Table 3). It was observed that mostly higher values of SL were associated with higher values of K_{sn}. Figure 6 depicts sudden changes in steepness with high K_{sn} occurring in the initial course of the Kabini, Bhavani, Noyil, and lower Cauvery Rivers, respectively. However, similar situations were observed in the middle and lower courses of the Shimsha River, and in the initial along with a lower course of the Hemavathi River. The Hemavathi, Shimsha, and Bhavani Rivers exhibited higher K_{sn} values also in their middle courses, while the Kabini, Noyil, and lower Cauvery Rivers showed higher K_{sn} values only in their initial courses. For the Kabini, Bhavani, Noyil, and lower Cauvery Rivers, relatively minor variations in K_{sn} were observed in their downstream courses. Specifically, in the Hemavathi River, a sudden change in steepness occurred at an approximate elevation of 790 m and a distance of 105 km from the source of the river. For the Bhavani River, an increase in the K_{sn} was observed approximately 10 km from the source of the river, at an elevation of approximately 1900 m. However, for the Shimsha River, high K_{sn} were observed both at the mouth (elevation 580 m) and in the middle course of the river (elevation 710 m). These observations highlight the diverse geomorphic characteristics and different patterns of fluvial erosion within the Cauvery basin, which is also governed by the diverse ranges of HI and SL. Distinct changes in K_{sn} were observed corresponding to features such as rapids, waterfalls, and dams. Conversely, low SL values were associated with low values of the K_{sn}, denotes relatively flat terrain with plain or peneplain features, which are conducive to agricultural and settlement practices. The presence of step-like appearance along the steepness profile suggests the alternating presence of hard and soft rocks, formed through erosional activity (Stalin and Achyuthan, 2014). Relatively high SL values corresponded to the locations of waterfalls, dams, rapids, and falls along the river courses in all six sub-basins (Table 4). This occurrence of waterfalls and dams in old topography (lower value of HI) may indicate past river rejuvenation resulting from relative sea level falls (Ramkumar et al., 2003, Ramkumar et al., 2019, Nagendra and Reddy, 2017). The locations of the higher SL values along with the range of K_{sn} values in all sub-basins were investigated using high-resolution Google Earth images (Table 4) and the results for the Shimsha and lower Cauvery Rivers are displayed (Figure 7 and 8), respectively.

Table 3. Distribution of knickpoints in different sub-basins

Knickpoints	Total number	30-500	500-1000	1000-2000	2000-4000	4000-8000	8000-62000	62000-161000	Maximum SL value (gradient meters)	Maximum K_{sn} range
Hemavathi	393	385	4	4	0	0	0	0	1951	>42
Kabini	279	278	1	0	0	0	0	0	655	>48
Shimsha	469	422	27	7	4	4	5	0	61,545	>36
Bhavani	3162	2190	440	289	150	60	30	3	160,884	75-90
Noyil	1260	798	197	145	75	34	11	0	15,548	35-42
Lower Cauvery	257	210	10	14	16	5	2	0	11,530	20-25

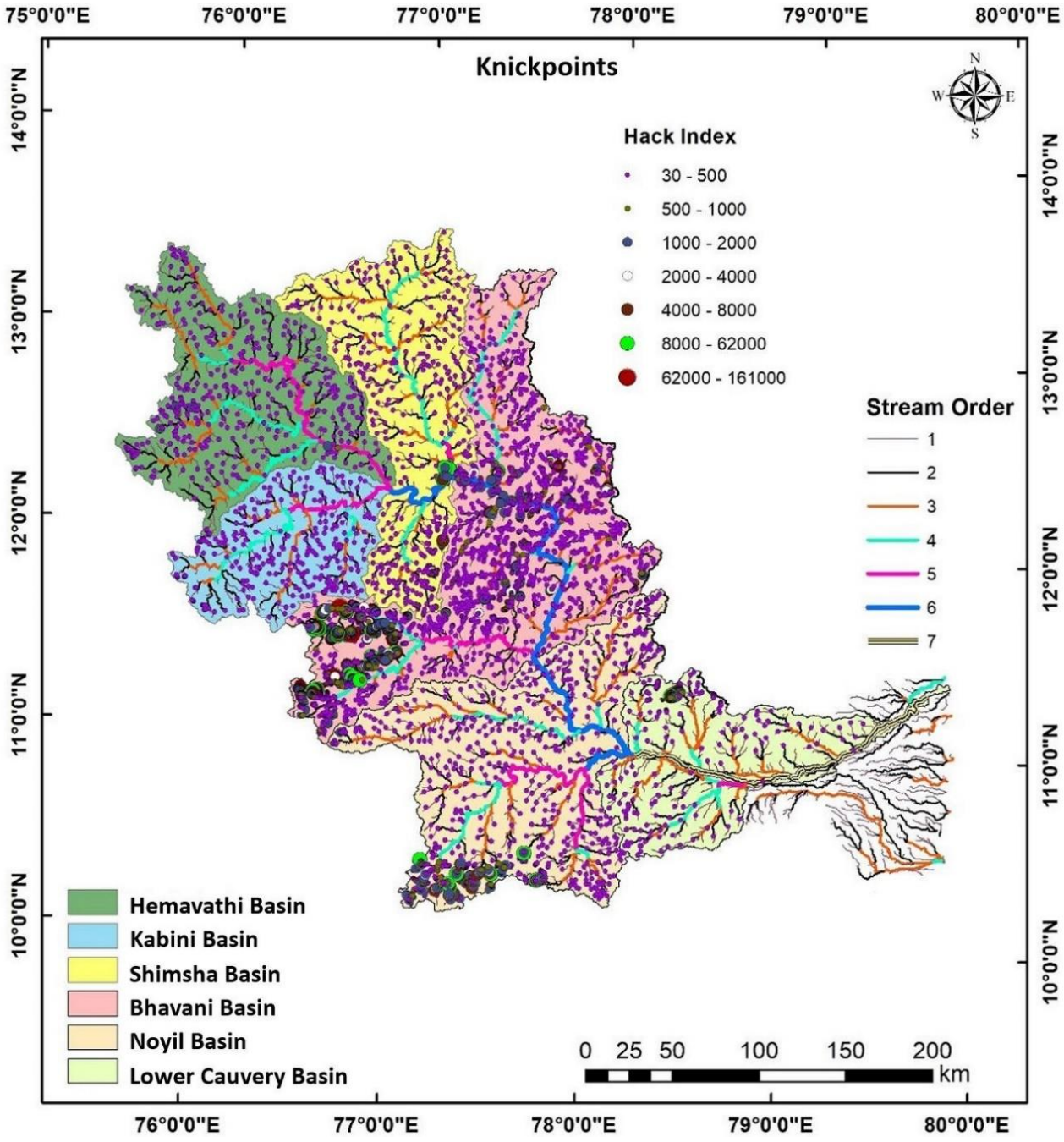

Figure 5. Spatial distribution of knickpoints calculated using the Hack index across the Cauvery basin

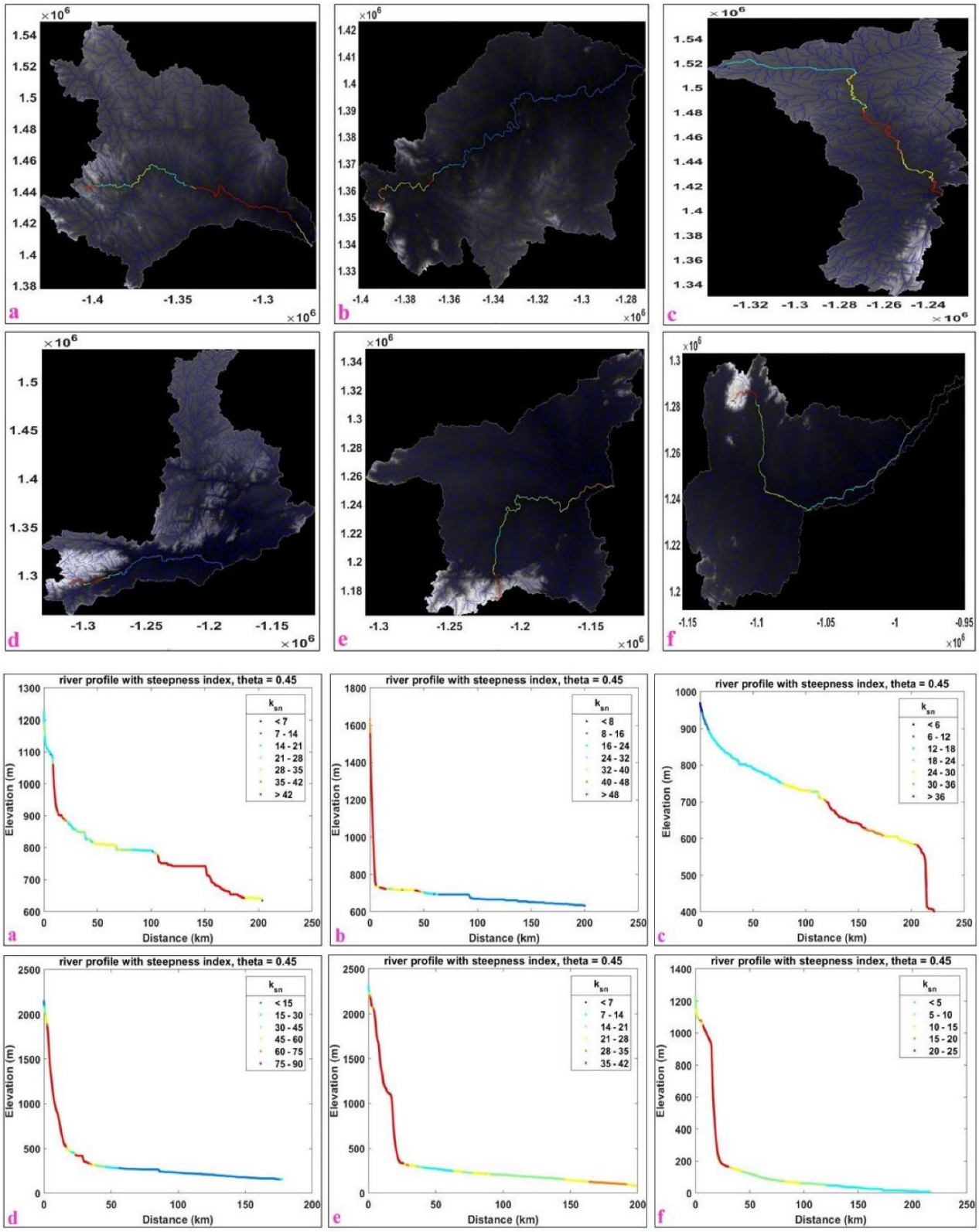

Figure 6. Normalized channel steepness index profiles for rivers with the highest value of knickpoints: **a)** Hemavathi, **b)** Kabini, **c)** Shimsha, **d)** Bhavani, **e)** Noyil, and **f)** Lower Cauvery

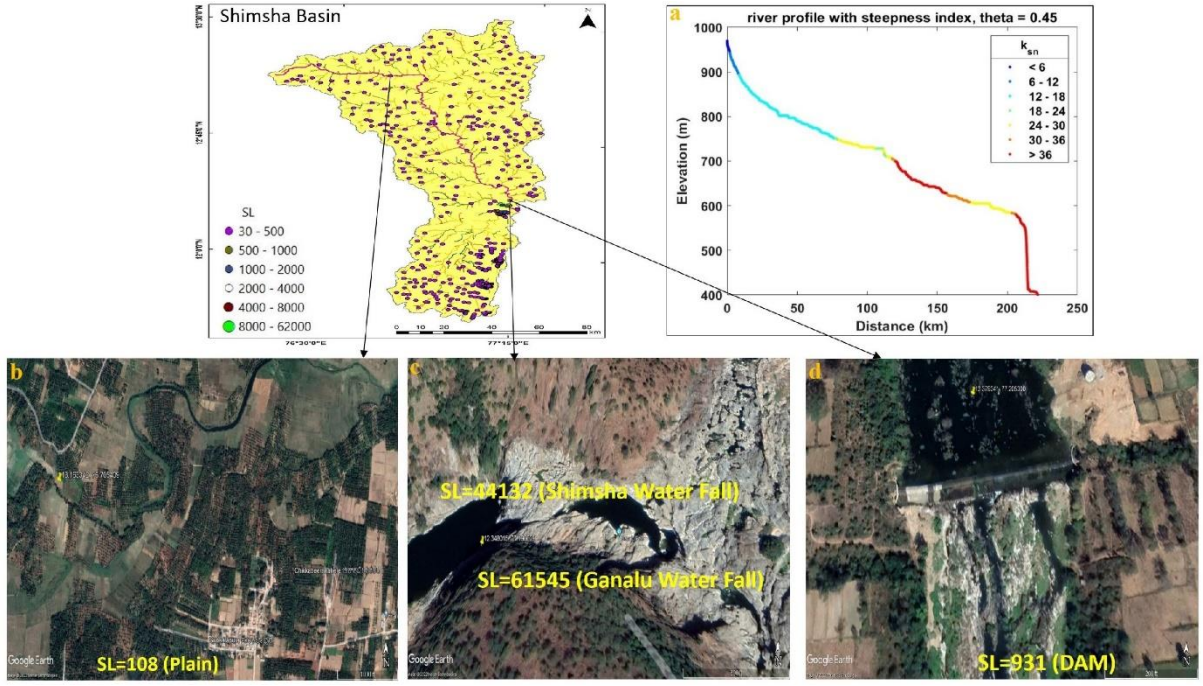

Figure 7. Interpretation of geomorphic indices (SL and K_{sn}) for the Shimsha basin: **a)** K_{sn} profile, **b)** low SL value, **c)** and **d)** high SL value

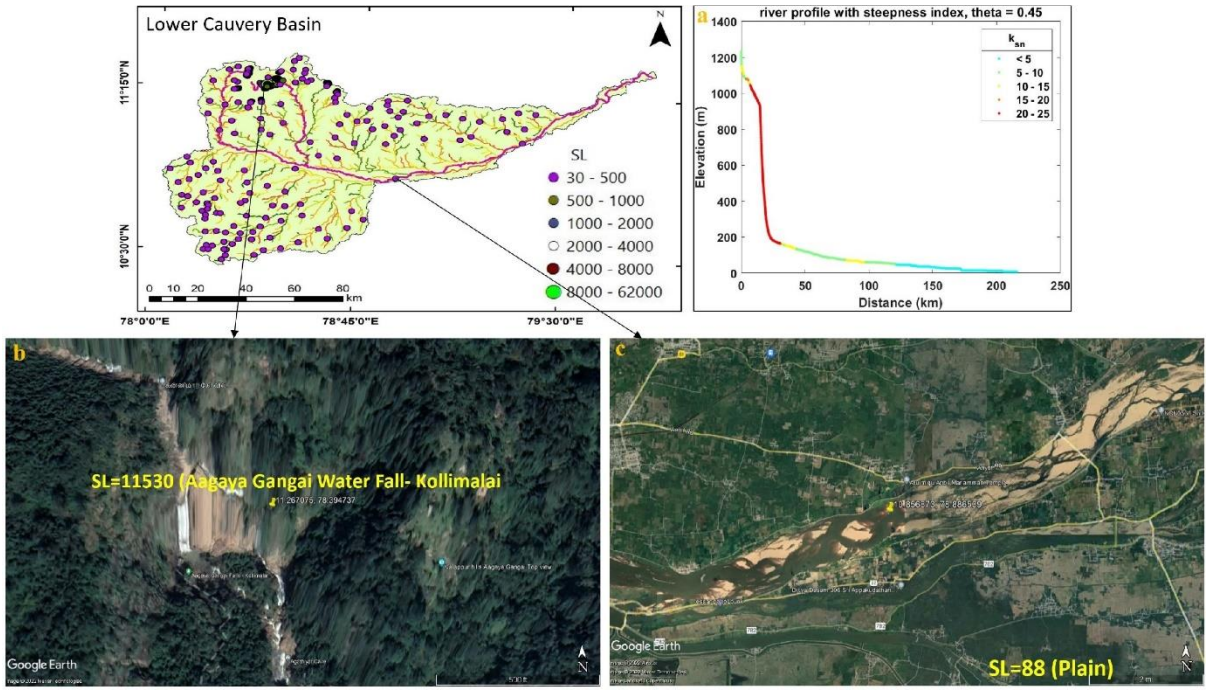

Figure 8. Interpretation of geomorphic indices (SL and K_{sn}) for the Lower Cauvery basin: **a)** K_{sn} profile, **b)** high SL value, **c)** low SL value

The maximum SL value of 61,545 and 11,530 gradient meters were computed for the Shimsha and lower Cauvery Rivers respectively with an elevation interval of 30 meters. Particularly high values (61,545 and 44,132) were observed near the mouth of the Shimsha River over the Ganalu and Shimsha waterfalls respectively (Figure 7). Figure 7(d) shows the high SL value of 931 corresponds to the dam along the river. Similarly, the significantly high value (11,530) near the initial course of the lower Cauvery River corresponds to the Aagaya Gangai falls in Kollimalai (Figure 8). These locations with high SL values also exhibited correspondingly high values of the K_{sn}, indicating steep terrain features. Specifically, the maximum K_{sn} range values were >36 and 20-25 for the Shimsha and lower Cauvery Rivers, respectively. Conversely, low values of the K_{sn} denote featureless, flat topography, as evidenced by low SL values of 108 and 88 for the Shimsha and lower Cauvery Rivers, respectively

Table 4. Interpretation of significantly high values of the SL and K_{sn} indices

Basins	SL value (gradient meter)	Interpretation	Range of K_{sn}
Hemavathi	1951	KRS DAM	>42
	1606	Water Fall	>42
Kabini	655	Undulating Terrain	>48
Shimsha	61545	Ganalu Water Fall	>36
	44132	Shimsha Water Fall	24-30
	38087	Gaganachukki Water Fall	18-24
	13889	Water Fall	24-30
	931	DAM	24-30
Bhavani	160884	Fall (Dry)	75-90
	31432	Pilloor DAM	75-90
	22992	Sigur Water Fall	75-90
	18568	Chunchi Water Fall	75-90
	14739	Catherine Water Fall	75-90
	12279	Moyar Water Fall	75-90
	12203	Kullakamby Water Fall	75-90
Noyil	15548	Water Fall	35-42
	11707	Water Fall	35-42
	8861	Thalakuthu Water Fall	35-42
	7791	Polur Water Fall	35-42
	6661	Pulla Veli Water Fall	35-42
	5798	Chilandhiyar Water Fall	35-42
Lower Cauvery	11530	Aagaya Gangai Water Fall	20-25
	5233	Water Fall	20-25

4.4 Integrated Analysis of Geomorphic Indices with Landform Features

The present study explores the relationship between extracted geomorphic indices and classified landform features to assess the influence of extracted geomorphic parameters on the topography of the Cauvery basin. Landform feature extraction was conducted using TPI and slope position classification into 10 distinct classes (Figure 9). The areal percentage cover for each landform feature across all six sub-basins of the Cauvery River were estimated, with analysis showed in Table 5. Each sub-basin shows varying proportions of landform types, indicating the diverse geomorphic characteristics within the basin. The observations show that the plain/peneplain feature occupied the highest percentage area across all sub-basins with open slopes being the second type of landform, except for the lower Cauvery basin. The lower Cauvery basin exhibited the highest percentage of area covered by plains (89.39%), followed by the Noyil (83.24%), and Shimsha (82.30%) basins. However, the Bhavani basin contained the lowest percentage of plain area (52.15%) among all sub-basins, while the Hemavathi and Kabini basins contained 64.60% and 62.53% plain area, respectively. The percentage cover of open slope landform features was highest for the Bhavani basin (21.08%) and lowest for the lower Cauvery basin (1.48%), similarly for the upper slopes (3.71% and 0.69%, respectively) also. The largest percentage area of deeply incised streams and high ridges were observed in the Bhavani basin (4.18% and 5.75%), representing significant topographic variations while the smallest areas were observed in the lower Cauvery basin (1.82% and 2.24%). The areal percentage cover of local ridges/hills in valleys was relatively low compared to other classes, followed by upland drainages. Valleys covered the highest percentage in the Bhavani basin (4.82%) and the lowest in the Shimsha basin (1.96%). The percentage of midslope drainages and midslope ridges/small hills in plains was highest for the Kabini basin (4.51% and 4.18%) and lowest for the lower Cauvery basin (1.23% and 0.51%), respectively.

Peneplains/plains were the most extensive landform features across all six sub-basins, with the lower Cauvery basin exhibiting the highest areal coverage (89.39%), followed by the Noyil basin (83.24%). These sub-basins exhibited low HI values of 0.11 and 0.12, along with very low K_{sn} values at their end courses (Figure 6), indicating the presence of monadnock features. However, the Bhavani basin had a lower areal coverage of plain area (52.15%), correlating with its relatively high HI value (0.22), highest SL value (160,884 gradient meters) and number of knickpoints (3162) among all sub-basins (Table 3). Anomalous behavior was observed in the Shimsha basin, which had a high percentage of plain area (82.30%), but also the largest HI value of 0.27. This anomaly may be attributed to upliftment in this basin relative to sea level fall (Ramkumar et al., 2003, Ramkumar et al., 2019, Nagendra and Reddy, 2017), accelerating erosion activity and forming waterfalls, dams, and rapids near the basin mouth, supported by the second-highest SL value (61,545 gradient meters) in this basin (Table 3). The Hemavathi basin also had relatively less areal coverage (64.60%) for the plain area and a high HI value of 0.22. High ridge features occupied the highest coverage (5.75%) in the Bhavani basin, which had the highest number of

knickpoints (3162) and a relatively high HI value (0.22), suggesting the most rugged terrain in the Cauvery basin with the minimum plain area (52.15%). However, high ridge feature had minimal areal coverage in the lower Cauvery basin (2.24%), which had a low HI value (0.11) and the minimum number of knickpoints (257), indicating an extensive plain area (89.39%). The presence of deeply incised streams features in the basin (Table 5) can be linked to upliftment relative to sea level, and accelerating erosion activity (Raju et al., 1994, Stalin and Achyuthan, 2014, Nagendra and Reddy, 2017). It was observed that low HI values, fewer knickpoints, SL, and K_{sn} indices corresponding to relatively plain areas, while high values of these indices corresponded to undulating terrain.

The presence of rugged terrain characterized by high values of SL and K_{sn} index indicates areas of intense erosional activity and topographic variability. Waterfalls and dams were associated with higher values of geomorphic indices. The relatively high HI values suggest a mature landscape and extensive erosion. Overall, the integrated analysis highlights the intricate relationship between geomorphic indices and landform features in shaping the topography and landscape evolution of the studied basin.

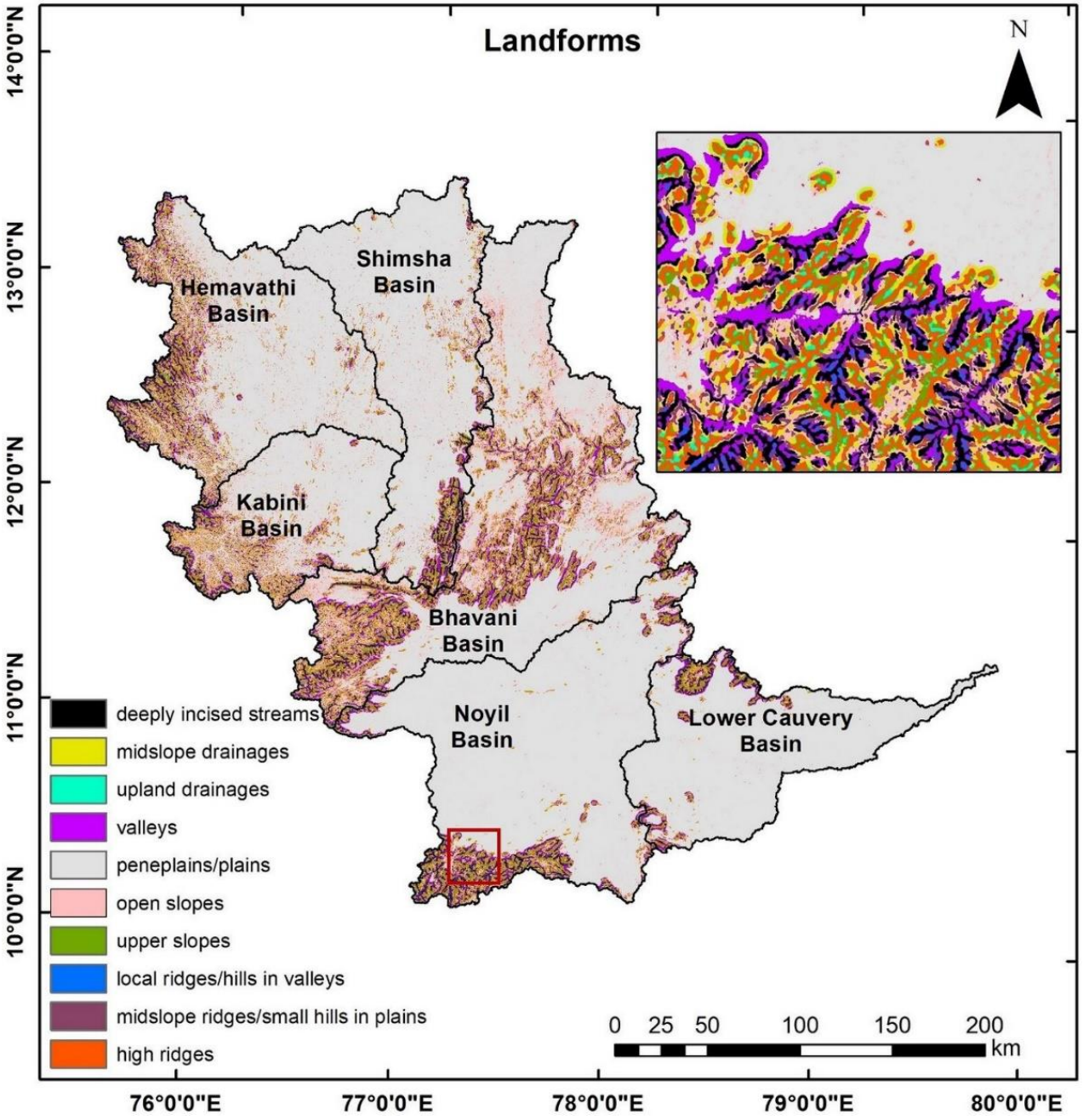

Figure 9. Landform classification map for the Cauvery basin

Table 5. Areal percentage distribution of landform features

Landforms	Hemavathi (area in % cover)	Kabini (area in % cover)	Shimsha (area in % cover)	Bhavani (area in % cover)	Noyil (area in % cover)	Lower Cauvery (area in % cover)
Deeply incised streams	3.41	2.71	1.87	4.18	2.63	1.82
Midslope drainages	3.91	4.51	1.89	4.07	1.75	1.23
Upland drainages	0.41	0.39	0.42	0.39	0.55	0.45
Valleys	2.91	2.61	1.96	4.82	2.48	2.07
Peneplains/plains	64.60	62.53	82.30	52.15	83.24	89.39
Open slopes	13.55	16.84	5.67	21.08	3.47	1.48
Upper slopes	2.70	1.98	1.27	3.71	1.42	0.69
Local ridges/hills in valleys	0.19	0.12	0.13	0.17	0.21	0.12
Midslope ridges/ small hills in plains	3.99	4.18	1.50	3.68	1.14	0.51
High ridges	4.33	4.13	2.99	5.75	3.11	2.24
Total	100	100	100	100	100	100

5. Conclusions

Landscape characterization is essential for studying geomorphic evolution and resource managements in river basins. By integrating computed geomorphic indices with classified landform features, the present study provides an understanding of spatial variations in fluvial erosion across the Cauvery River Basin. The computed indices show an old, eroded, and dissected topography, with HI values ranging from 0.11 to 0.27. Bhavani and Hemavathi sub-basins show similar HI values (0.22), but demonstrate different erosional processes and geomorphic maturity, showing the spatial heterogeneity within the basin. High SL values-up to 160,884 gradient meters in the Bhavani basin-along with numerous knickpoints (3162) and elevated K_{sn} values (90), indicate zones of intense incision, steep slopes, and lithological transitions, often coinciding with waterfalls and anthropogenic structures such as dams. Conversely, low SL values (e.g., 108 and 88) and peneplain features (up to 89.39% in lower Cauvery) indicate flat, stable landscapes. These spatial patterns suggest that the Bhavani basin is one of the most dynamically evolving sub-regions, while the lower Cauvery represents a geomorphically subdued terrain. Clustering of knickpoints at elevations between 0-120 m above sea level implies that Quaternary sea-level fluctuations played a significant role in river rejuvenation. This integrative approach enhances geomorphic interpretation, and may give a valuable framework for sediment management, water resource planning, and land-use policy. Future studies could incorporate terrace chronology or dated sea-level curves to further test the sea-level linkage and refine models of long-term fluvial evolution in peninsular India.

Acknowledgments

We thank Shri Nilesh M. Desai, Director, SAC, Dr. R.P. Singh, Director, IIRS Dehradun, Dr. Rashmi Sharma, Deputy Director, EPSA, Dr. R.B. Upadhyaya, Group Head, PGSG, and Sri. Jayaprasad P, Head, Geosciences division for allowing carrying out this research work.

Author contributions

Conceptualization, S.R. and R.A.; Data curation, S.R.; Formal analysis, S.R.; Investigation, S.R. and R.A.; Methodology, S.R.; Visualization, S.R. and R.A.; writing-original draft preparation, S.R.; Supervision, R.A. and D.R.R.; Validation, R.A. and D.R.R.; writing-review and editing, R.A.; Project administration, D.R.R.; Resources, D.R.R.

Declarations

Funding No funding was received for conducting this study.

Data availability Data will be made available on reasonable request from the corresponding author.

Ethical approval Not applicable.

Competing interests The authors have no competing interests to declare that are relevant to the content of this article.

References

Adediran, A.O., I. Parcharidis, M. Poscolieri and K. Pavlopoulos (2004). Computer-assisted discrimination of morphological units on north-central Crete (Greece) by applying multivariate statistics to local relief gradients. Geomorphology, 58, 357–370. http://dx.doi.org/10.1016/j.geomorph.2003.07.024

Alexandrowicz, Z. (1994). Geologically controlled waterfall types in the Outer Carpathians. Geomorphology,

9(2), 155–165. https://doi.org/10.1016/0169-555X(94)90073-6

Anderson, R.S. and S.P. Anderson (2010). Geomorphology. Cambridge University Press, Cambridge. https://doi.org/10.1017/CBO9780511794827

Bishop, P., T.B. Hoey, J.D. Jansen and I.L. Artza (2005). Knickpoint recession rate and catchment area: the case of uplifted rivers in eastern Scotland. Earth Surface Processes and Landforms, 30(6), 767–778. https://doi.org/10.1002/esp.1191

Blaszczynski, J.S. (1997). Landform characterization with geographic information systems. Photogrammetric Engineering and Remote Sensing, 53(2), 183–191.

Bull, W.B. (2007). Tectonic geomorphology of mountains: A new approach to paleoseismology. Blackwell Publishing Ltd., Oxford, 316 p. https://doi.org/10.1002/9780470692318

Burbank, D.W. and R.S. Anderson (2011). Tectonic geomorphology, second ed. John Wiley & Sons, Ltd, Chichester, UK. https://doi.org/10.1002/9781444345063

Central Water Commission (1989). Major River Basins of India – An overview. Ministry of Water Resources, Government of India, New Delhi.

Coates, D.R. (1958). Quantitative geomorphology of small drainage basins of southern Indiana. Technical Report no. 10, Project NR 389-042, Office of Naval Research, Geography Branch. Department of Geology, Columbia University, New York.

Das, S., A. Gupta and S. Ghosh (2017). Exploring groundwater potential zones using MIF technique in a semi-arid region: A case study of Hingoli district, Maharashtra. Spatial Information Research, 25(6), 749–756. https://doi.org/10.1007/s41324-017-0144-0

Das, S., S.D. Pardeshi, P.P. Kulkarni and A. Doke (2018). Extraction of lineaments from different azimuth angles using geospatial techniques: A case study of Pravara Basin, Maharashtra, India. Arabian Journal of Geosciences, 11, 160. https://doi.org/10.1007/s12517-018-3522-6

Das, S. and S.D. Pardeshi (2018b). Comparative analysis of lineaments extracted from Cartosat, SRTM and ASTER DEM: A study based on four watersheds in the Konkan region, India. Spatial Information Research, 26(1), 47–57. https://doi.org/10.1007/s41324-017-0155-x

Das, S. and S.D. Pardeshi (2018a). Morphometric analysis of Vaitarna and Ulhas river basins, Maharashtra, India: Using geospatial techniques. Applied Water Science, 8(6), 158. https://doi.org/10.1007/s13201-018-0801-z

Das, S. (2018). Geographic information system and AHP-based flood hazard zonation of Vaitarna Basin, Maharashtra, India. Arabian Journal of Geosciences, 11(19), 576. https://doi.org/10.1007/s12517-018-3933-4

Das, S. (2018). Geomorphic characteristics of a bedrock river inferred from drainage quantification, longitudinal profile, knickzone identification and concavity analysis: A DEM-based study. Arabian Journal of Geosciences, 11, 680. https://doi.org/10.1007/s12517-018-4039-8

Dikau, R., E.E. Brabb and R.M. Mark (1991). Landform classification of New Mexico by computer (No. 91-634). U.S. Department of the Interior, U.S. Geological Survey. https://doi.org/10.3133/ofr91634

Dikau, R. (1989). The application of a digital relief model to landform analysis. In: J.F. Raper (ed), Three-dimensional applications in geographic information systems. Taylor and Francis, London, pp. 51–77. https://doi.org/10.1201/9781003069454-5

Dusan, B., B. Jan, K. Daniel and B. Lenka (2017). Morphometric and geological conditions for sediment accumulation in the Udava River, Outer Carpathians, Slovakia. Journal of Geographical Sciences, 27(8), 981–998. https://doi.org/10.1007/s11442-017-1416-2

Etchebehere, M.L.C., A.R. Saad, V.J. Fulfaro and J.A.J. Perinotto (2004). Aplicação do índice "Relação Declividade–Extensão – RDE" na Bacia do Rio do Peixe (SP) para detecção de deformações neotectônicas. Revista do Instituto de Geociências USP, Série Científica, 4(2), 43–56. https://doi.org/10.5327/S1519-874X2004000200004

Etchebehere, M.L.C., A.R. Saad, G. Santoni, F.C. Casado and V.J. Fulfaro (2006). Detecção de prováveis deformações neotectônicas no vale do Rio do Peixe, região ocidental paulista, mediante aplicação de índices RDE (Relação Declividade–Extensão) em segmentos de drenagem. Revista UNESP Geociências, 25(3), 271–287.

Gailleton, B., S.M. Mudd, F.J. Clubb, D. Peifer and M.D. Hurst (2019). A segmentation approach for the reproducible extraction and quantification of knickpoints from river long profiles. Earth Surface Dynamics, 7(1), 211–230. https://doi.org/10.5194/esurf-7-211-2019

García, A.F., Z. Zhu, T.L. Ku, O.A. Chadwick and J. Chacon Montero (2004). An incision wave in the geologic record: Alpujarran corridor, southern Spain (Almería). Geomorphology, 60(1–2), 37–72. https://doi.org/10.1016/j.geomorph.2003.07.012

Gregory, K.J. (1966). Dry valley and the composition of the drainage net. Journal of Hydrology, 4, 327–340. https://doi.org/10.1016/0022-1694(66)90096-5

Guisan, A., S.B. Weiss and A.D. Weiss (1999). GLM versus CCA spatial modeling of plant species distribution. Plant Ecology, 143(1), 107–122. https://doi.org/10.1023/A:1009841519580

Hack, J.T. (1973). Stream-profile analysis and stream-gradient index. Journal of Research of the U.S. Geological Survey, 1, 421–429.

Hayakawa, Y.S. and T. Oguchi (2006). DEM-based identification of fluvial knickzones and its application to Japanese mountain rivers. Geomorphology, 78(1–2), 90–106. https://doi.org/10.1016/j.geomorph.2006.01.018

Horton, R.E. (1932). Drainage basin characteristics. Transactions of the American Geophysical Union, 13(1), 350–361. https://doi.org/10.1029/TR013i001p00350

Horton, R.E. (1945). Erosional development of streams and their drainage basins: Hydrophysical approach to quantitative morphology. Bulletin of the Geological Society of America, 56(3), 275–370. https://doi.org/10.1130/0016-7606(1945)56[275:EDOSAT]2.0.CO;2

Howard, A.D. and G. Kerby (1983). Channel changes in badlands. Geological Society of America Bulletin, 94(6), 739–752. https://doi.org/10.1130/0016-7606(1983)94%3C739:CCIB%3E2.0.CO;2

Howard, A.D., W.E. Dietrich and M.A. Seidl (1994). Modeling fluvial erosion on regional to continental scales. Journal of Geophysical Research, 99(B7), 13971–13986. https://doi.org/10.1029/94JB00744

Howard, A.D. (1994). A detachment-limited model of drainage basin evolution. Water Resources Research, 30(7), 2261–2285. https://doi.org/10.1029/94WR00757

Huang, X. and J.D. Niemann (2006). An evaluation of the geomorphically effective event for fluvial processes over long periods. Journal of Geophysical Research: Earth Surface, 111(F3). https://doi.org/10.1029/2006JF000477

Jaiswara, N.K., S.K. Kotluri, P. Pandey and A.K. Pandey (2020). MATLAB functions for extracting hypsometry, stream-length gradient index, steepness index, chi gradient of channel, and swath profiles from digital elevation model (DEM) and other spatial data for landscape characterization. Applied Computing and Geosciences, 7, 100033. https://doi.org/10.1016/j.acags.2020.100033

Jenness, J. (2006). Topographic Position Index (tpi_jen.avx) extension for ArcView 3.x, v. 1.3a. Jenness Enterprises. http://www.jennessent.com/arcview/tpi.htm

Keller, E.A. and N. Pinter (2002). Active tectonics, earthquakes, uplift and landscape, 2nd edn. Prentice Hall, Upper Saddle River, 362 p.

Kirby, E. and K.X. Whipple (2012). Expression of active tectonics in erosional landscapes. Journal of Structural Geology, 44, 54–75. https://doi.org/10.1016/j.jsg.2012.07.009

Kumar, A., S.K. Samuel and V. Vyas (2015). Morphometric analysis of six subwatersheds in the central zone of Narmada River. Arabian Journal of Geosciences, 8, 5685–5712. https://doi.org/10.1007/s12517-014-1655-9

Lambeck, K., H. Rouby, A. Purcell, Y. Sun and M. Sambridge (2014). Sea level and global ice volumes from the Last Glacial Maximum to the Holocene. Proceedings of the National Academy of Sciences of the United States of America. https://doi.org/10.1073/pnas.1411762111

Langbein, W.B. (1947). Topographic characteristics of drainage basins. U.S. Geological Survey Water-Supply Paper, 968-C, 125–157. https://doi.org/10.3133/wsp968C

Lewis, W.V. (1945). Nick points and the curve of water erosion. Geological Magazine, 82(6), 256–266. https://doi.org/10.1017/S0016756800082108

Manu, M.S. and S. Anirudhan (2008). Drainage characteristics of Achankovil River basin, Kerala. Journal of the Geological Society of India, 71(6), 841–850. https://www.geosocindia.org/index.php/jgsi/article/view/80780

Marple, R.T. and P. Talwani (1993). Evidence of possible tectonic upwarping along the South Carolina coastal plain from an examination of river morphology and elevation data. Geology, 21(7), 651–654. https://doi.org/10.1130/0091-7613(1993)021%3C0651:EOPTUA%3E2.3.CO;2

Martinez, M., E. Hayakawa, J.C. Stevaux and J.D. Profeta (2011). SL index as an indicator of anomalies in the longitudinal profile of the Pirapó River. Revista Geociências, 30(1), 63–76.

McKeown, F.A., M. Jones-Cecil, B.L. Askew and M.B. McGrath (1988). Analysis of stream-profile data and inferred tectonic activity, Eastern Ozark Mountains region. U.S. Geological Survey Bulletin, 1807, 39. https://doi.org/10.3133/b1807

Merrits, D. and T. Hesterberg (1994). Stream networks and long-term surface uplift in the New Madrid seismic zone. Science, 265(5175), 1081–1084. https://doi.org/10.1126/science.265.5175.1081

Meybeck, M., P. Green and C. Vorosmarty (2001). A new typology for mountains and other relief classes. Mountain Research and Development, 21(1), 34–45. https://doi.org/10.1659/0276-4741(2001)021[0034:ANTFMA]2.0.CO;2

Miller, J.R. (1991). The influence of bedrock geology on knickpoint development and channel-bed degradation along downcutting streams in south-central Indiana. Journal of Geology, 99(4), 591–605. https://doi.org/10.1086/629519

Miller, V.C. (1953). A quantitative geomorphic study of drainage basin characteristics in the Clinch Mountain area, Virginia and Tennessee. Department of Geology, Columbia University, New York, pp 389–402.

Moglen, G.E. and R.L. Bras (1995). The effect of spatial heterogeneities on geomorphic expression in a model of basin evolution. Water Resources Research, 31(10), 2613–2623. https://doi.org/10.1029/95WR02036

Mokarram, M. and A. Seif (2014). GIS-based automated landform classification in Zagros mountain (case study: Grain mountain). Bulletin of Environmental Pharmacology and Life Sciences, 3(3), 20–32.

Montgomery, D.R., T.B. Abbe, J.M. Buffington, N.P. Peterson, K.M. Schmidt and J.D. Stock (1996). Distribution of bedrock and alluvial channels in forested mountain drainage basins. Nature, 381, 587–589. https://doi.org/10.1038/381587a0

Mudd, S.M., M. Attal, D.T. Milodowski, S.W.D. Grieve and D.A. Valters (2014). A statistical framework to quantify spatial variation in channel gradients using the integral method of channel profile analysis. Journal of Geophysical Research: Earth Surface, 119(2), 138–152. https://doi.org/10.1002/2013JF002981

Nagendra, R. and A.N. Reddy (2017). Major geologic events of the Cauvery Basin, India and their correlation with global signatures – A review. Journal of Palaeogeography, 6(1), 69–83. https://doi.org/10.1016/j.jop.2016.09.002

Pedrera, A., J.V. Pérez-Peña, J. Galindo-Zaldívar, J.M. Azañón and A. Azor (2009). Testing the sensitivity of geomorphic indices in areas of low-rate active folding (eastern Betic Cordillera, Spain). Geomorphology, 105(3–4), 218–231. https://doi.org/10.1016/j.geomorph.2008.09.026

Pérez-Peña, J.V., J.M. Azañón and A. Azor (2009). CalHypso: an ArcGIS extension to calculate hypsometric curves and their statistical moments. Applications to drainage basin analysis in SE Spain. Computers and Geosciences, 35(6), 1214–1223. https://doi.org/10.1016/j.cageo.2008.06.006

Perron, J.T. and L. Royden (2013). An integral approach to bedrock river profile analysis. Earth Surface Processes and Landforms, 38(6), 570–576. https://doi.org/10.1002/esp.3302

Pike, R.J. (1999). A bibliography of geomorphometry, the quantitative representation of topography, Supplement 3 (Open-File Report 99-140). U.S. Geological Survey. https://doi.org/10.3133/ofr99140

Queiroz, G., E. Salamuni and E. Nascimento (2015). Knickpoint finder: A software tool that improves neotectonic analysis. Computers and Geosciences, 76, 80–87. https://doi.org/10.1016/j.cageo.2014.11.004

Raju, D.S.N., B.C. Jaiprakash, C.N. Ravindran, R. Kalyanasunder and P. Ramesh (1994). The magnitude of hiatus and sea level changes across the K–T boundary in Cauvery and Krishna Godavari Basin. Journal of the Geological Society of India, 44(3), 301–315.

Ramkumar, M., M. Santosh, S.A. Rahaman, A. Balasundareshwaran, K. Balasubramani, M. Mathew, B. Sautter, N. Siddiqui, P. Usha, K. Sreerhishya, G. Prithiviraj, R. Nagarajan, T. Venugopal, D. Menier and K. Kumaraswamy (2019). Tectono-morphological evolution of the Cauvery, Vaigai, and Thamirabarani river basins: Implications on timing, stratigraphic markers, relative roles of intrinsic and extrinsic factors, and transience of Southern Indian landscape. Geological Journal, 54(5), 1–42. https://doi.org/10.1002/gj.3520

Ramkumar, M., D. Stüben and Z. Berner (2003). Lithostratigraphy, depositional history, and sea level changes of the Cauvery Basin, southern India. Geological Annals of the Balkan Peninsula, 65(1), 1–27. https://doi.org/10.2298/GABP0301001M

Saadat, H., R. Bonnell, F. Sharifi, G. Mehuys, M. Namdar and S. Ale-Ebrahim (2008). Landform classification from a digital elevation model and satellite imagery. Geomorphology, 100(3), 453–464. https://doi.org/10.1016/j.geomorph.2008.01.011

Schmidt, J. and A. Hewitt (2004). Fuzzy land element classification from DTMs based on geometry and terrain position. Geoderma, 121(3–4), 243–256. https://doi.org/10.1016/j.geoderma.2003.10.008

Schoenbohm, L., K. Whipple, B. Burchfiel and L. Chen (2004). Geomorphic constraints on surface uplift, exhumation, and plateau growth in the Red River region, Yunnan Province, China. Bulletin of the Geological Society of America, 116(7–8), 895–909. https://doi.org/10.1130/B25364.1

Schumm, S.A. (1956). Evolution of drainage systems and slopes in badlands at Perth Amboy, New Jersey. Bulletin of the Geological Society of America, 67(5), 597–646. https://doi.org/10.1130/0016-7606(1956)67[597:EODSAS]2.0.CO;2

Seeber, L. and V. Gornitz (1983). River profiles along the Himalayan arc as indicators of active tectonics. Tectonophysics, 92(4), 335–367. https://doi.org/10.1016/0040-1951(83)90201-9

Snyder, N.P., K.X. Whipple, G.E. Tucker and D.J. Merritts (2000). Landscape response to tectonic forcing: digital elevation model analysis of stream profiles in the Mendocino triple junction region, Northern California. Bulletin of the Geological Society of America, 112(8), 1250–1263. https://doi.org/10.1130/0016-7606(2000)112%3C1250:LRTTFD%3E2.0.CO;2

Sreedevi, P.D., K. Subrahmanyam and A. Shakeel (2005). The significance of morphometric analysis for obtaining groundwater potential zones in a structurally controlled terrain. Environmental Geology, 47(3), 412–420. https://doi.org/10.1007/s00254-004-1166-1

Stalin, M. and H. Achyuthan (2014). Cauvery River: Late Quaternary fluvial process and landforms. Geophysical Research Abstracts, 16, EGU2014-16266.

Strahler, A.N. (1952). Hypsometric (area-altitude) analysis of erosional topography. Bulletin of the Geological Society of America, 63(11), 1117–1142. https://doi.org/10.1130/0016-7606(1952)63[1117:HAAOET]2.0.CO;2

Strahler, A.N. (1957). Quantitative analysis of watershed geomorphology. Transactions of the American Geophysical Union, 38(6), 913–920. https://doi.org/10.1029/TR038i006p00913

Sun, C., T. Wan, X. Xie, X. Shen and K. Liang (2016). Knickpoint series of gullies along the Luoyunshan Piedmont and its relation with fault activity since late Pleistocene. Geomorphology, 268(1–2), 266–274. https://doi.org/10.1016/j.geomorph.2016.06.026

Thomas, J., S. Joseph, K.P. Thrivikramji and G. Abe (2011). Morphometric analysis of the drainage system and

its hydrological implication in the rain shadow region, Kerala, India. Journal of Geographical Sciences, 21(6), 1077–1088. https://doi.org/10.1007/s11442-011-0901-2

Weiss, A. (2001). Topographic position and landforms analysis. In: Poster presentation, ESRI User Conference, San Diego, CA.

Whipple, K.X., G.S. Hancock and R.S. Anderson (2000). River incision into bedrock: mechanics and relative efficacy of plucking, abrasion, and cavitation. Bulletin of the Geological Society of America, 112(3), 490–503. https://doi.org/10.1130/0016-7606(2000)112%3C490:RIIBMA%3E2.0.CO;2

Whipple, K.X. and G.E. Tucker (1999). Dynamics of the stream-power river incision model: implications for height limits of mountain ranges, landscape response timescales, and research needs. Journal of Geophysical Research, 104(B8), 17661–17674. https://doi.org/10.1029/1999JB900120

Whipple, K.X. (2004). Bedrock rivers and the geomorphology of active orogens. Annual Review of Earth and Planetary Sciences, 32(1), 151–185. https://doi.org/10.1146/annurev.earth.32.101802.120356

Willgoose, G. and G. Hancock (1998). Revisiting the hypsometric curve as an indicator of form and process in transport-limited catchment. Earth Surface Processes and Landforms, 23(7), 611–623. https://doi.org/10.1002/(SICI)1096-9837(199807)23:7%3C611::AID-ESP872%3E3.0.CO;2-Y

Wobus, C., K.X. Whipple, E. Kirby, N. Snyder, J. Johnson, K. Spyropolou, B. Crosby and D. Sheehan (2006). Tectonics from topography: procedures, promise, and pitfalls. Geological Society of America Special Paper, 398, 55–74. https://doi.org/10.1130/2006.2398(04)

Wohl, E.E., D.M. Thompson and A.J. Miller (1999). Canyons with undulating walls. Bulletin of the Geological Society of America, 111(7), 949–959. https://doi.org/10.1130/0016-7606(1999)111%3C0949:CWUW%3E2.3.CO;2

Zaprowski, B. J., E. B. Evenson, F. J. Pazzaglia and J. B. Epstein (2001). Knickzone propagation in the Black Hills and northern High Plains: a different perspective on the late Cenozoic exhumation of the Laramide Rocky Mountains. Geology, 29(6), 547–550. http://dx.doi.org/10.1130/0091-7613(2001)029%3C0547:KPITBH%3E2.0.CO;2